9

Biocytin-Based Contrast Agents for Molecular Imaging: An Approach to Developing New *In Vivo* Neuroanatomical Tracers for MRI

Anurag Mishra[1,4] et al.[*]
[1]*Department for Physiology of Cognitive Processes, Max-Planck Institute for Biological Cybernetics, Tübingen,*
[4]*Department of Chemistry, Durham University, South Road, Durham*
[1]*Germany*
[4]*England*

1. Introduction

One of the most striking characteristic of the brain is its profuse neuronal connectivity. Not surprisingly, the function of the nervous system critically depends on the spatiotemporal pattern of intercommunication between different regions of the brain. Both macro- and microscopic aspects of the wiring diagrams of brain circuits are relevant and need to be understood in order to cope with the complexity of the brain function. In this way, for instance, the long-range connections that carry the functional specification of cortical territories need to be studied together with the detailed microcircuits inside a cortical column. Moreover, the temporal dimension of these wiring diagrams must be investigated since neuronal networks are dynamic structures exhibiting context-dependent changes in synaptic weights (Canals et al., 2009) and numbers (Chklovskii et al., 2004). Investigations over the last decades strongly suggest that stimulus or task related neural activity is distributed over large parts of the brain, covering different cortical and sub-cortical areas. For a detailed understanding of brain function, it is of prime importance to understand the organization of the neuronal connections. To chart the anatomical connections between the various components of brain networks, the neuronal tract tracing technique has been proved to be very useful. Thus, experimental tools that allow the exploration of brain circuits at

[*]Kirti Dhingra[1,5], Ritu Mishra[2,6], Almut Schüz[1], Jörn Engelmann[2], Michael Beyerlein[1], Santiago Canals[1,7] and Nikos K. Logothetis[1,3]
[1]*Department for Physiology of Cognitive Processes, Max-Planck Institute for Biological Cybernetics, Tübingen, Germany*
[2]*High-Field MR Center, Max-Planck Institute for Biological Cybernetics, Tübingen, Germany*
[3]*Imaging Science and Biomedical Engineering, University of Manchester, Manchester, England*
[4]*Department of Chemistry, Durham University, South Road, Durham, England*
[5]*Case Center for Imaging Research, Department of Radiology, Case Western Reserve University, Cleveland, OH, USA*
[6]*School of Biological & Biomedical Sciences, Durham University, South Road, Durham, England*
[7]*Instituto de Neurociencias CSIC-UMH, Campus de San Juan, San Juan de Alicante, Spain*

diverse organizational levels are mandatory for the understanding of brain intercommunication and information processing.

Magnetic Resonance Imaging (MRI) has great potential for mapping brain connectivity (Koretsky and Silva, 2004). It is a noninvasive volume imaging technique that can be applied longitudinally to the same subject, capturing the temporal dimension of brain connections and providing complete descriptions of large-scale three-dimensional (3-D) neuronal networks. The main limitation of MRI is its low sensitivity. To compensate for weak signals in MRI, efforts have been focused on the development of MR contrast agents. Recently, the paramagnetic ion manganese (Mn^{2+}) has been introduced as a MR-contrast agent for investigating *in vivo* neuronal connectivity (Canals et al., 2008; Pautler et al., 1998). Following the general mechanism of other classical anterograde tracers, Mn^{2+} is taken up by neurons and transported to the distant synaptic terminals where it accumulates and reveals the projection fields (Canals et al., 2008; Leergaard et al., 2003; Murayama et al., 2006; Pautler et al., 1998; Saleem et al., 2002; Sloot and Gramsbergen, 1994; Tjalve et al., 1995; Van der Linden et al., 2002; Watanabe et al., 2004), thus delineating brain connectivity. In contrast to classical tracers, which require processed fixed tissue for data analysis, neuronal tracing with Mn^{2+} as an MR tracer is performed *in vivo*.

However, cellular toxicity is an important drawback that challenges the applicability of Mn^{2+}-enhanced MRI (MEMRI). It has been shown that Mn^{2+} can be cytotoxic at concentrations used for neural tracing (Canals et al., 2008; Chandra et al., 1981; McMillan, 1999; Pal et al., 1999). Additional disadvantages of this technique are its high diffusion at the injection site, which challenge the specificity of the resulting projections, and its incompatibility with other visualization systems (Canals et al., 2008). If Mn^{2+} toxicity is not counteracted, it generates such perturbations in the neuronal circuits under study that eliminate the advantage of using Mn^{2+} as an *in vivo* neuronal tracer. In addition, at the end of an *in vivo* connectivity experiment using a paramagnetic tracer, it could be very informative to analyze the laminar and subcellular distribution of the neuronal connections. Such an experiment cannot be performed by using current MEMRI methods. New non-toxic paramagnetic tracers with anterograde, but also retrograde capabilities (i.e. when the tracer moves from the terminal ends to the soma identifying the origin of a synaptic contact) are desirable, particularly for functional studies, for quantitative 3-D analysis of connectivity, or for repetitive applications investigating the same pathway dynamically over time.

Here we report a strategy to produce neuronal tract tracers with paramagnetic properties, biochemical stability and biocompatibility. The new tracers are imbued with double functionality in a single molecule that allows both *in vivo* longitudinal brain connectivity studies by means of MRI and postmortem subcellular investigation in the same experimental animal. Therefore, the macro- and microscopic aspects of a brain circuit can be simultaneously investigated.

As a proof of concept we focused on the well-known neuroanatomical tracer biocytin which is taken up by neurons and transported in both antero- and retrograde directions (King et al., 1989). Several characteristics make biocytin a good tracer model. It has been used in numerous tracing studies, both after intracellular or extracellular application, and much is known about its biophysical properties (Horikawa and Armstrong, 1988). Due to its high affinity to avidin, it can be visualized by using a host of avidin conjugated markers at the light- and electron microscopic level. Extracellular application of biocytin results in very well localized injection sites with no uptake by fibers of passage or glial cells. These two last

characteristics result in a high specificity of biocytin tracings (Kita and Armstrong, 1991; Lapper and Bolam, 1991; Wirsig-Wiechmann, 1994).

Structurally, biocytin consists of D-Biotin and L-lysine connected via an amide bond which is susceptible to cleavage by biotinidase enzyme. Biotinidase is the enzyme mainly responsible for recycling of the vitamin biotin by cleaving biocytin and biotinylated peptides/proteins (Hymes and Wolf, 1996; Mock et al., 1999; Wilbur et al., 1996). Biotinidase plays an important role in brain function (Pispa, 1965; Suchy et al., 1985). A deficiency in the biotinidase enzyme has been linked to several neurological disorders (Heller et al., 2002; Tsao and Kien, 2002; Zaffanello et al., 2003). For this reason, biocytin has relatively small half life *in vivo*, which forces short post injection survival times and increases the probability of only partial reconstruction of neuronal projections. Using the same strategy, we recently introduced two new biocytin-based neuroanatomical tracers [*aminopropyl-biocytin* and *serine-biocytin*; Scheme 1] with improved enzymatic stability (Mishra et al., 2009). The *in vivo* results for these two derivatives of biocytin demonstrated that they are biochemically stable conjugates, retain full tracing capabilities and more importantly these molecules allow longer post-injection survival times due to the improved stability and therefore, provide more detailed and complete connectivity information. The commercial biocytin was totally degraded 96 h postinjection, however, these improved neuronal tracers still stained neuronal cell bodies and fibers at the injection site and remote terminal fields. These improved neuronal tracers present an edge over conventional histological procedures, as their better stability could reduce the problems related to the endogenous degradation of the tracer molecule before the animal is sacrificed. As was suggested in the previous work (Mishra et al., 2009), the applicability of these new agents could be further diversified by coupling with different reporter moieties and utilized for multimodal tracing. For instance, the combination of reported molecules with MR reporters could serve as a tool for magnetic resonance imaging and, hence, be used for visualizing brain connectivity *in vivo*.

Here in, we have followed up our previous investigations and developed two novel and structurally distinct gadolinium (Gd^{3+}) containing biocytin-based multimodal neuronal tracers ([**Gd.L^1**] and [**Gd.L^2**]) (Scheme 1). The backbone of these structures were functionalized by covalently linking the kinetically stable gadolinium caged organic macrocyclic moiety [DOTA and DO3A-serine] as MR reporters to perform *in vivo* longitudinal brain connectivity studies by means of MRI, leaving α-position of lysine moiety free for internalization in neurons and biotin moiety free for avidin binding for subsequent visualization with postmortem microscopic histological methods.

The first MR tracer **[Gd.L^1]** was derived from the recently published stable biocytin variant *aminopropyl-biocytin* (Mishra et al., 2009), whereby [Gd.DOTA] was coupled to *aminopropyl-biocytin* via an amide bond. The second MR tracer, **[Gd.L^2]** consists of a new precursor [Gd.DO3A-serine] which has an orthogonal amine and a carboxylate group on the fourth nitrogen of [Gd.DO3A] for the coupling of biotin and lysine, respectively. By replacing [Gd.DOTA] with FITC in **[Gd.L^1]** fluorescently labeled *aminopropyl-biocytin* **[Fluo.L^1]** was obtained for fluorescence microscopy studies.

We present data that demonstrate the validity of the approach by showing cortical connectivity *in vivo* applying T_1-weighted MR-imaging. In addition, the corresponding subcellular details, fibers and neuronal morphology under light microscopy were investigated in the same experimental animals by means of avidin-biotin interactions and conventional histological techniques.

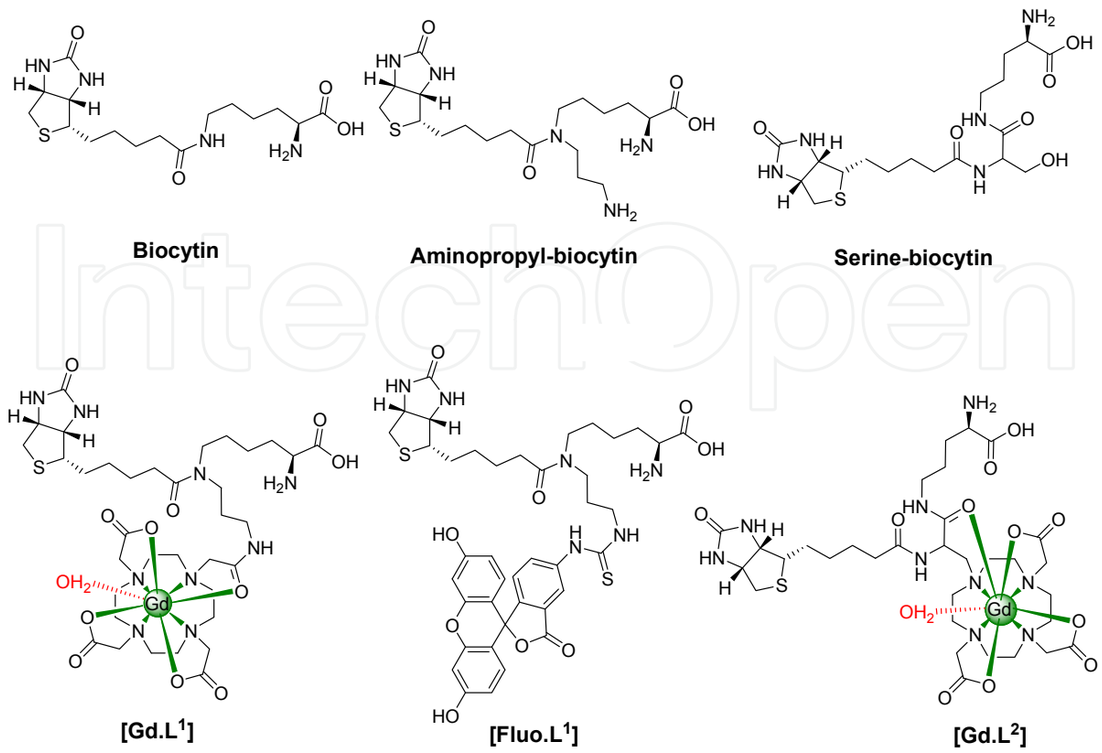

Scheme 1. Structures of studied biocytin-derived neuroanatomical tracers.

2. Results and discussion

2.1 Synthesis of ligands and complexes

Two structurally different Gd^{3+} complexing neuroanatomical tracers (**[Gd.L¹]** and **[Gd.L²]**; Scheme 1) were designed and synthesized. These conjugates enclosed the [Gd.DO3A] construct as an MR reporter and biotin to be used for microscopic visualization by means of histological techniques.

The first MR tracer **[Gd.L¹]** was derived from stable biocytin variant, propylamine-biocytin (Mishra et al., 2009), where [Gd.DOTA] was coupled to aminopropyl-biocytin via amide bond. **[Gd.L¹]** was synthesised in seven steps prior to complexation with Gd^{3+} (Scheme 2). Propylamine-biocytin **6** was synthesized in three steps, starting with the reaction of acrylonitrile on $^{\alpha}N$-carbobenzyloxy-L-lysine methyl ester giving cyano compound **4**. Propinonitrile derivative **5** was obtained after coupling acid D-biotin with the secondary amine of **4** by using PyBroP as a coupling reagent and diisopropylethylamine as the base in anhydrous CH_2Cl_2. Subsequent selective reduction of nitrile groups in the presence of Ra-Ni, H_2, 7M NH_3/MeOH yielded amine intermediate **6**. The macrocycle intermediate **3** (tris-*tert*-butyl-DOTA) was obtained in two steps by stepwise alkylation of tris-*tert*-butyl-DO3A, **1**, with benzylbromoacetate in acetonitrile generating **2,** and following deprotection of benzyl groups produced the corresponding acid **3** in high yield (Pope et al., 2003). Then, tetra-ester **7** was synthesized by coupling of amine **6** and acid **3** [EDC/HOBt/NMM] in anhydrous DMF, from which **L¹** was obtained by successive deprotections (benzylcarbamate removal by hydrogenation using Pd-C as the catalyst, methyl group with LiOH and *tert*-butyl groups with neat TFA).

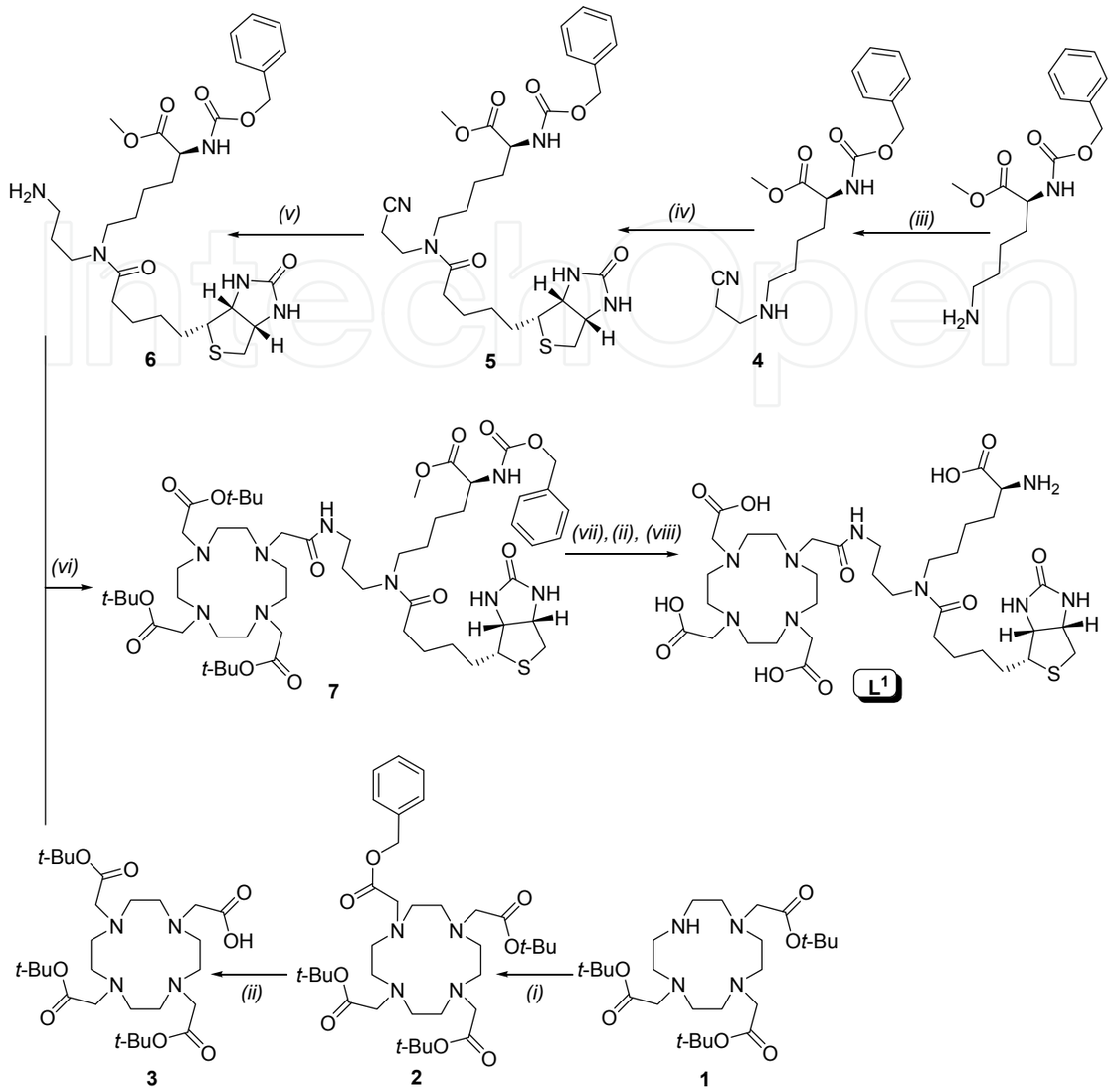

Scheme 2. Reagents and conditions: *(i)* benzylbromoacetate, MeCN, K_2CO_3, 100°C; *(ii)* Pd-C (10%), H_2, MeOH, 50 psi; *(iii)* acrylonitrile, TEA, MeOH; *(iv)* Biotin, PyBroP/DIPEA/CH_2Cl_2; *(v)* Ra-Ni, H_2, 7 M NH_3/MeOH, 50 psi; *(vi)* NMM/EDC/HOBt/DMF; *(vii)* LiOH, THF:MeOH:water (3:2:2); *(viii)* TFA (neat).

The second MR tracer, **[Gd.L²]** consists [Gd.DO3A-serine] which has an orthogonal amine and a carboxylate group available on the fourth nitrogen of [Gd.DO3A] for the coupling of biotin and lysine, respectively. **[Gd.L²]** was synthesized in 9 steps prior to complexation with Gd^{3+} (Scheme 3). Bromination on the hydroxyl group of *N*-carbobenzyloxy-L-serine methyl ester yielded **8**. The bromination reaction was run for no more than 30 min. This avoided the formation of allyl analogues of the product by elimination of bromine. The most reasonable route to synthesize ligand **10** was by alkylation of **8** on **1** but the elimination of the bromine group under highly basic conditions resulted in starting compound together with allyl side product. An alternative route was taken to obtain **10** where monoalkylated intermediate **9** was generated by alkylation of excess cyclen with **8** in anhydrous toluene,

which was further alkylated by *tert*-butylbromoacetate yielding **10**. Mono-acid **11** was obtained by mild hydrolysis of the methyl ester in the presence of LiOH, which was further coupled to amine of Boc-Lys-OMe [EDC/HOBt/NMM] in anhydrous DMF to produce **12**. The benzylcarbamate was hydrogenated over Pd/C to yield the secondary amine **13** which was coupled to acid D-biotin [EDC/HOBt/NMM] in anhydrous DMF to give tetra-ester **14**.

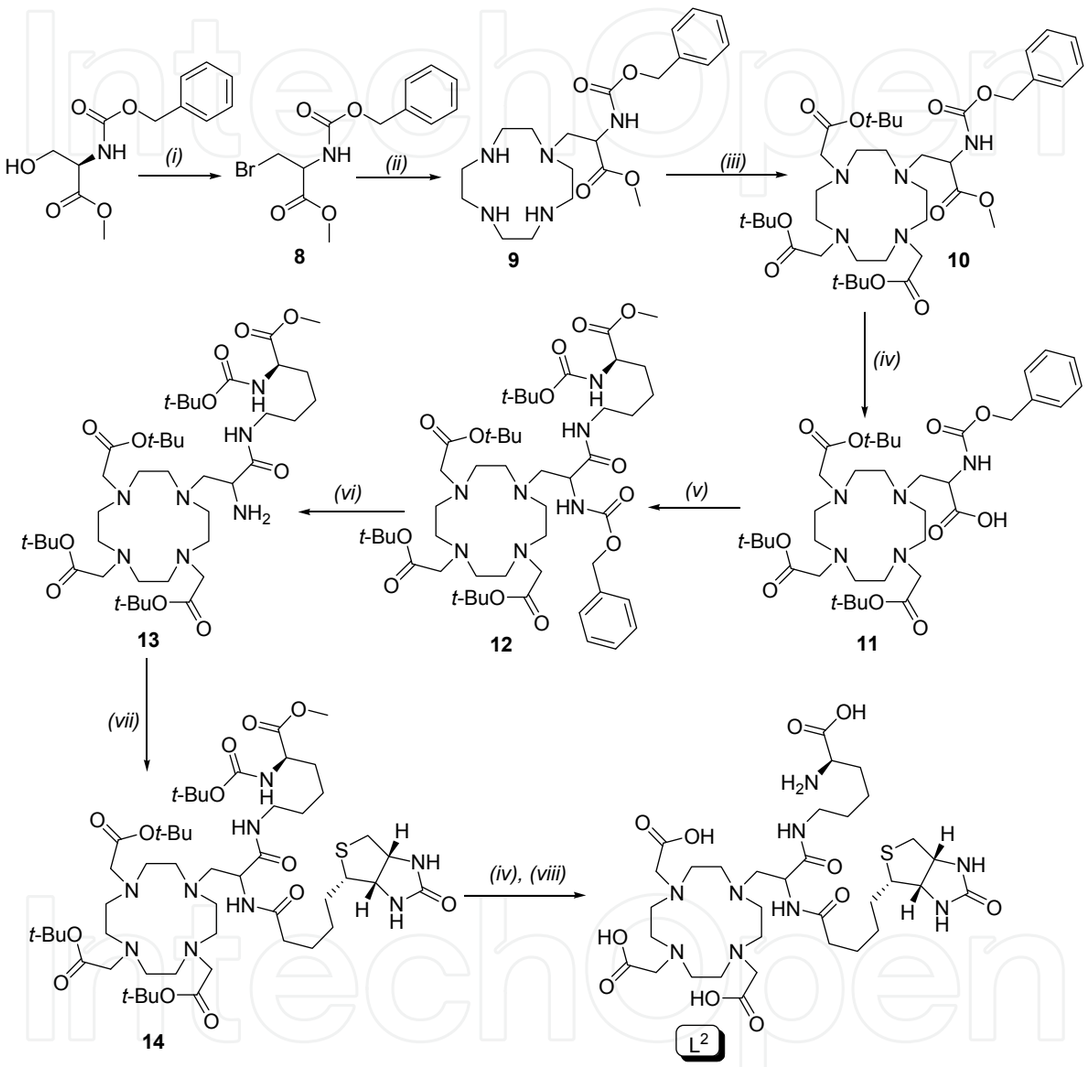

Scheme 3. Reagents and conditions: *(i)* NBS/PPh_3/DMF; *(ii)* cyclen/toluene; *(iii) tert*-butyl bromoacetate/Na_2CO_3/MeCN; *(iv)* LiOH, THF:MeOH:H_2O (3:2:2); *(v)* Boc-Lys-OMe, NMM/HOBt/EDC/DMF; (*vi*) Pd-C (10%), H_2, MeOH, 50 psi; *(vii)* biotin, HATU/DIPEA/DMF; *(viii)* TFA (neat).

Carboxylic acid derivative **L²** was obtained by successive deprotections (first the methyl group with LiOH and then *tert*-butyl groups with neat TFA).
Ligands, **L¹** and **L²,** were purified by RP-HPLC and loaded with Gd^{3+} using $GdCl_3.6H_2O$ in water at pH 6.5. The final concentration of Gd^{3+} was determined by inductively-coupled plasma optical emission spectrophotometry (ICP-OES).

2.2 Proton relaxivity modulation of [Gd.L^1] and [Gd.L^2] by biotin-avidin interaction

The extensive applications of biotin-avidin interactions have been found attractive in biomolecule detection, medical diagnostics, immunoassays and nanoscience (Bickel et al., 2001; Cao et al., 2003; Caswell et al., 2003; Rivera et al., 2003; Weizmann et al., 2003). Due to the high affinity of biotin to tetrameric avidin, biotinylated compounds can be visualized by light microscopy in postmortem tissues using avidin-conjugated markers. To investigate and quantify the binding behavior of the two contrast agents (CAs) to avidin which is important for the histological detection, we performed MRI experiments at 7T (300 MHz) [phosphate buffered saline (PBS), 7.4 pH, 23°C] with increasing concentrations of avidin proportional to constant concentrations of CAs (0.25 mM) and measured the proton longitudinal relaxivities (r_{1p}).

The proton longitudinal relaxivities (r_{1p}) of **[Gd.L^1]** and **[Gd.L^2]** at 7T (300 MHz) [phosphate buffered saline (PBS), 7.4 pH, 23°C] were found to be 5.52±0.08 mM^{-1} s^{-1} and 7.27±0.13 mM^{-1} s^{-1}, respectively. As anticipated, **[Gd.L^1]** shows similar relaxivity to [Gd.DOTA] complexes. However **[Gd.L^2]** shows higher relaxivity than that reported in the literature for Gd-DO3A derivatives in such a physiological solution (Caravan et al., 1999). The observed higher relaxivity in solution is explained by the high molecular volume and a significant second-sphere contribution through amide moieties close to the paramagnetic proximity present in the molecule (Aime et al., 1996; Botta, 2000).

Complexes	r_{1p} ($mM^{-1}s^{-1}$)		Change (%)
	[Gd.L^n]	**[Gd.L^n]:avidin**	
[Gd.L^1]	5.52±0.08	6.10±0.11	**+**11
[Gd.L^2]	7.27±0.13	6.65±0.09	-9

Table 1. Relaxivity (r_{1p}, mM^{-1}s^{-1}) for **[Gd.L^1]/[Gd.L^2]** and **[Gd.L^1]/[Gd.L^2]:avidin** complexes (23°C, 7T (300 MHz), pH 7.4, PBS, 0.25 mM complex).

Inevitable, r_{1p} of **[Gd.L^1]** was slightly increased (11%) in contrast to **[Gd-L^2]** (9% decreased) upon binding to avidin (Table 1). This is in reference to the Solomon–Bloembergen–Morgan theory envisaging that at high magnetic fields, the longitudinal proton relaxivity changes with the opposite of molecular rotational correlation time (τ_R) suggesting that relaxivity change should be expected upon binding of the CAs to macromolecules (Livramento et al., 2006). The saturation in r_{1p} at a ratio approximately at 2:1 (assuming a 2:1 stoichiometry of interaction) for the **[Gd-L^1]/[Gd-L^2]:avidin** adduct was obtained which clearly indicating similar steric hindrance of both CAs. These results suggest that **[Gd.L^1]** and **[Gd.L^2]** block the adjacent binding sites of biotin but evidently fit into two opposite binding pockets of avidin. The complexes {**[Gd.L^1]/[Gd.L^2]:avidin**} (2:1) binding stoichiometry reveal that **[Gd.L^1]** and **[Gd.L^2]** could be visualized by binding with avidin via histological techniques. However, an improved visualisation is expected if binding occurred to all pockets of avidin in a 4:1 ratio.

2.3 *In vitro* cell culture studies

It is well known from the literature that biocytin is a low molecular weight compound which has excellent uptake and transport capability in neuronal cells. Biocytin could be used as antero- as well as retrograde neuronal tract-tracer after intra- and extracellular injection in the brain (Kobbert et al., 2000). However, the uptake mechanism of biocytin at higher concentrations is not well known. A rapid and sodium/potassium-dependent high affinity uptake of biocytin in NB2a neuroblastoma cells was reported by Baur et al. This uptake was

very specific and selective to NB2a neuroblastoma cells as compared to C6 astrocytoma cells (Baur et al., 2002). Saturation kinetic of biocytin in a low concentration range was reported. However, the biocytin concentration in the brain is well below the reported concentration at half maximal saturation (K_m) of the biocytin uptake under physiological conditions (Baur et al., 2002). In contrast, after pressure or iontophoretic injection, local concentrations exceed the physiological concentration of biocytin manifold. Thus, the uptake mechanism under such conditions is not yet established.

The Gd-chelated macrocyclic modified biocytin molecules, [**Gd.L¹**] and [**Gd.L²**], are high molecular weight compounds as compared to biocytin alone. We investigated the cellular internalization of these compounds and their ability to enhance the MR contrast *in vitro*. For these studies murine N18 neuroblastoma cells were used as cellular model. In order to induce more neuronal metabolic and morphologic features in these tumor cells, serum deprivation was used to differentiate the cells (Marchisio et al., 1979). During the slow stepwise reduction of FBS content in the culture medium to 0.625% the growth rate slowed down and cells started to show a neuronal morphology with a network of neurite-like cellular processes which were completely absent at 10% FBS. Similar *in vitro* studies were also performed with the FITC containing *aminopropyl-biocytin* **[Fluo.L1]**. All cell incubations were performed in HBSS/10 mM HEPES buffer for 6 hours.

2.3.1 *In vitro* studies of cellular toxicity on N18 murine neuroblastoma cells

We first tested whether the contrast agents would have an adverse effect on differentiated N18 cells. For this purpose cells were incubated with [**Gd.L¹**] or [**Gd.L²**] for 6 h in HBSS/10 mM HEPES and the number of cells were determined by fluorescence spectroscopy using the DNA dye Bisbenzimid Hoechst 33342. Only [**Gd.L²**] showed a significant cytotoxic effect at 50 μM (Figure 1). Thus, all further experiments were done at concentrations below this level (40 and 20 μM for [**Gd.L¹**] and [**Gd.L²**]).

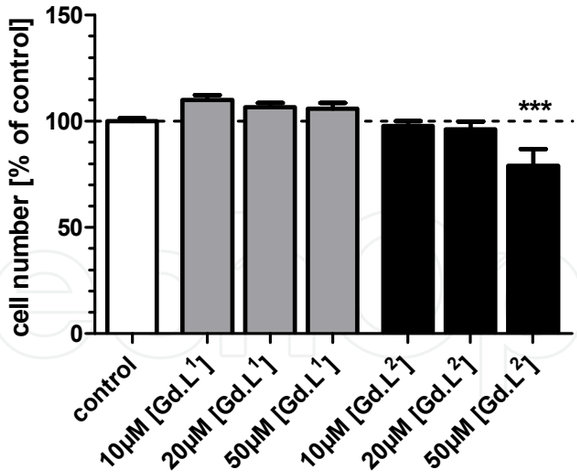

Fig. 1. Evaluation of the acute short term toxicity of [**Gd.L¹**] and [**Gd.L²**]. Differentiated N18 neuroblastoma cells were incubated with the indicated concentration of [**Gd.L¹**] or [**Gd.L²**] in HBSS/10 mM HEPES for 6h. Afterwards DNA dye Bisbenzimide Hoechst 33342 was added for 30 min in complete cell culture medium to determine the number of cells by the fluorescence of the dye/DNA conjugate (Ex 355nm/Em 465 nm). Values represent mean±SEM (n=6-12). ***p< 0.001, statistically different compared to control (ANOVA, Dunnett´s multiple comparison test).

2.3.2 Fluorescence microscopy to detect internalization and subcellular distribution

Since the intracellular distribution of [**Gd.L¹**] and [**Gd.L²**] cannot be directly detected by MRI, the fluorophore containing analogue to [**Gd.L¹**], [**Fluo.L¹**] was used. Fluorescence microscopy of living cells displayed a detectable uptake of the compound into morphologically differentiated N18 cells. Figure 2 shows the cellular localization of [**Fluo.L¹**] after incubation with 50 μM for 12 h and subsequent washing and quenching of remaining extracellular fluorescence by Trypan Blue. [**Fluo.L¹**] (green fluorescence of the covalently linked FITC) was internalized very quickly and mainly accumulated in vesicles in the perinuclear region (nuclei counterstained in blue) of the cells. Green fluorescence of [**Fluo.L¹**] could also be detected in the projections of the cells. These results indicate a predominantly endosomal uptake of [**Fluo.L¹**] into morphologically differentiated neuroblastoma cells. The optical evidence that [**Fluo.L¹**] was also detected along the processes of the cells set grounds for possible application of synthesized compounds as tract tracers.

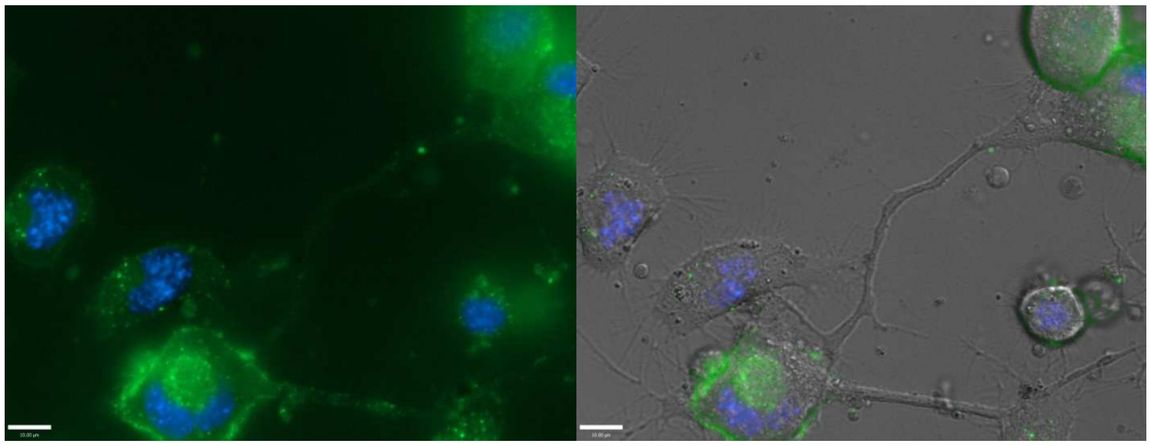

Fig. 2. Optical evidence for intracellular localization of [**Fluo.L¹**] in N18 neuroblastoma cells. Cells were incubated with 50 µM of [**Fluo.L¹**] for 6 h in HBSS/10 mM HEPES as described in materials and methods. Overlay of green (FITC in [**Fluo-L¹**]) and blue fluorescence (DNA dye Hoechst 33342) (left) and in addition of the phase contrast image (right).

2.3.3 MRI studies on N18 murine neuroblastoma cells

After proving the cellular uptake, the ability of [**Gd.L¹**] and [**Gd.L²**] to enhance contrast in MR images of labeled cells was tested. For this purpose differentiated N18 cells were incubated with either 20 or 40 µM of [**Gd.L¹**] or [**Gd.L²**], respectively. After removal of the incubation medium of all samples the labeled cells were extensively washed with buffer. A constant number of treated cells were transferred into 0.5 mL Eppendorf tubes and cells were allowed to settle down. T_1-weighted images were taken and the values of longitudinal (T_1) relaxation times were measured in an axial slice of cell pellets and supernatant at 3T and room temperature.

Figure 3 shows representative examples of T_1-weighted images achieved after incubation with 20 or 40 µM of [**Gd.L¹**] or 40 µM of [**Gd.L²**]. A significant contrast enhancement could be observed in the images for both compounds compared to control cells incubated in the absence of contrast agent. The determination of apparent cellular relaxation rate $R_{1,cell}$

(=1/$T_{1,cell}$) in the cell pellet confirmed these results (Figure 4). The significance levels here were lower since averages of independent experiments were taken.

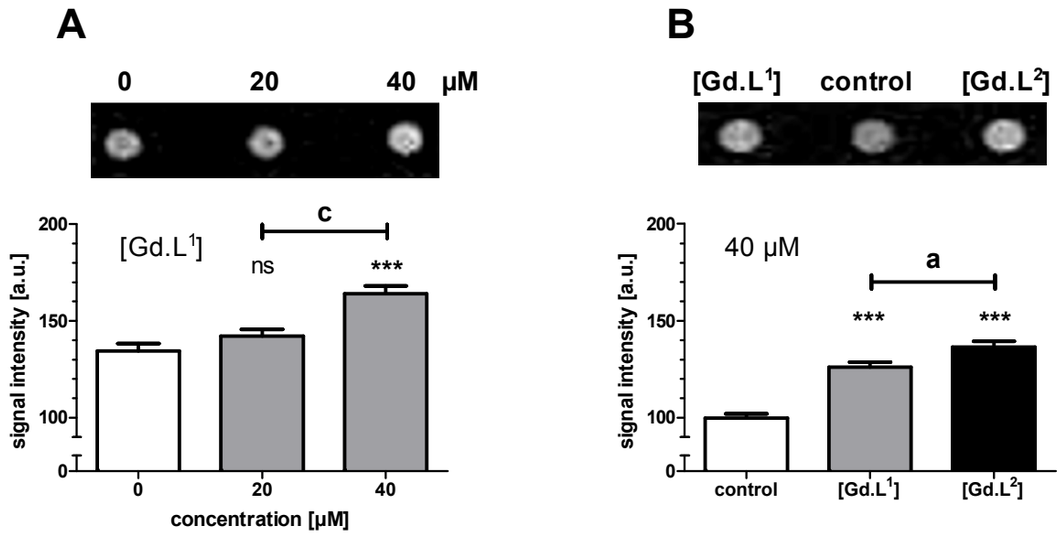

Fig. 3. Examples of T_1-weighted MR images of differentiated N18 neuroblastoma cells and analysis of the signal intensities in these images. Cells were incubated with 20 or 40 µM [**Gd.L¹**] (A) or 40 µM of [**Gd.L¹**] and [**Gd.L²**] (B) for 6 h in HBSS/10 mM HEPES. Cells were washed, trypsinized and resuspended in fresh culture medium (without CA) at a cell density of 1×10^7 cells/500 µL and transferred into 0.5 mL tubes. Cells were allowed to settle prior to MR experiments for imaging and determination of T_1 values in an axial slice through the cell pellet. Parameters for MRI are given in the experimental part. The bar graphs resulted from the pixelwise evaluation of signal intensity in the corresponding images. Values represent mean±SD (n=37 (A) and 44 (B)); ***, p>0.001, significantly different to control, a, p<0.05 and c, p>0.001, significant difference between 20 µM, 40 µM and [**Gd.L¹**], [**Gd.L²**], respectively (ANOVA, Tukey´s multiple comparison test).

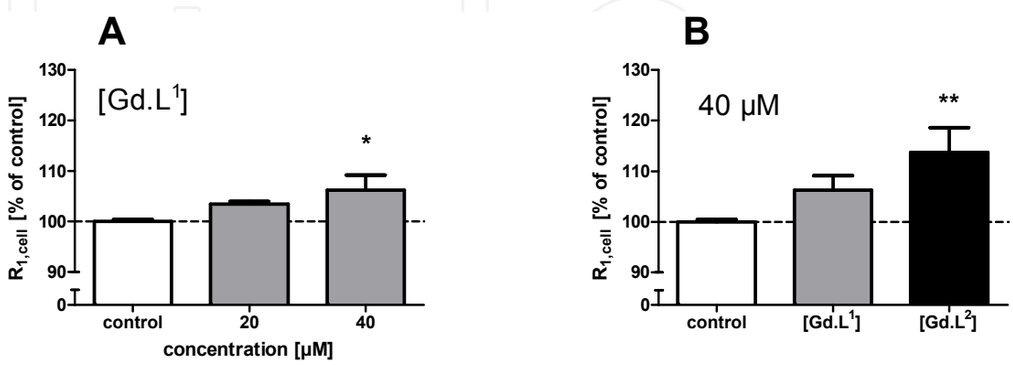

Fig. 4. Cellular relaxation rate $R_{1,cell}$ of differentiated N18 neuroblastoma cells. Values represent mean±SEM (n=2-5); **, p>0.01, *, p>0.05 significantly different to control (ANOVA, Dunnett´s multiple comparison test).

2.4 *In vivo* uptake and transport: MR and histology studies of [Gd.L^1] and [Gd.L^2] in rat brain

In the final step, we investigated the tracing abilities of these newly synthesized imaging probes, [**Gd.L¹**] and [**Gd.L²**], by means of MRI and classical histological methods in the same experimental animal. We performed a series of pressure and iontophoretic injections into the primary motor cortex (M1) of anaesthetized albino rats (Sprague Dawley) and evaluated the transport of these compounds at 24 and 48 h post-injection (see methods section for technical details). After the local injection of [**Gd.L¹**] in the primary motor cortex of the rat, the target area was visualized in T_1-weighted MRI as a large increase in signal (due to the decrease of the T_1 relaxation time; Figure 5A). Statistical analysis comparing baseline images (acquired either before or immediately after the injection) with images acquired after 24 and 48 h revealed a significant increase in T_1-weighted signal intensity in various brain regions

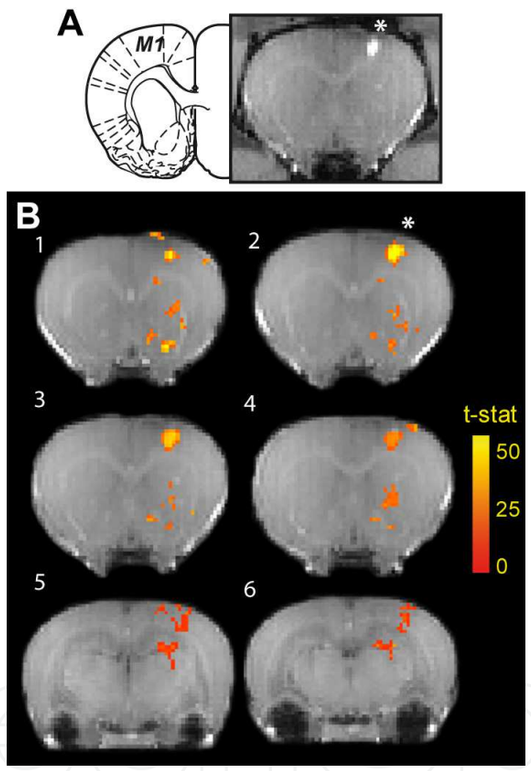

Fig. 5. *In vivo* neuronal tract tracing with **[Gd.L¹]**. Neuronal connections of the primary motor cortex M1 of the rat were investigated. (A) Coronal T_1-weighted images acquired 30 min after the injection of **[Gd.L¹]** in M1. Note the enhanced signal (asterisk) at the injection site. The inset shows a representative scheme of rat brain anatomy at the coordinates of the injection (Paxinos and Watson, 2007). (B) Shown are six coronal MR images illustrating the distribution of **[Gd.L¹]** signal in the brain after an injection in M1. The presence of signal is shown as statistical maps (unpaired t test; $p<0.01$) comparing the baseline (pre-injection scans) and scans acquired 48 h later, superimposed on the anatomical images. The results demonstrate local increases in signal due to **[Gd.L¹]** injection and long-range neuronal tract-tracing after 48 h in the striatum (1-4) and thalamus (5-6). After the last MRI session, the animal was euthanized and the histology is shown in Figure 6.

far away from the injection site. For instance, statistically significant increases in signal intensity were detected in the thalamus and the homologous contralateral M1 cortex (Figure 5B), areas that are well known to be connected with M1, suggesting that the tracer has actually been taken up by neurons *in vivo* and transported in the axons. This result corroborates the neuronal-tracing ability of [**Gd.L¹**] and its suitability for *in vivo* studies of brain connectivity. The MRI results obtained with [**Gd.L²**], after injection into the M1 cortex, showed a comparable pattern of neural connections as in [**Gd.L¹**] (data not shown).

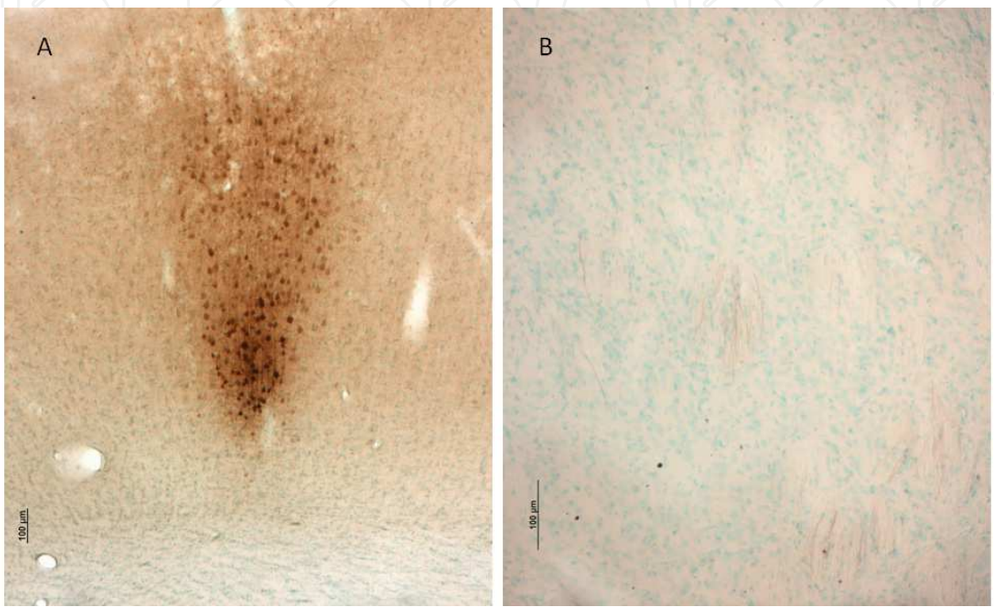

Fig. 6. Histological stain of the same brain as shown in Fig. 5, 48 h after an iontophoretic injection with [**Gd.L¹**]. Neurons at the injection site (A) have been stained. (B) Slightly stained fibres in the striatum bundles. The sections were counterstained with methyl green, visualizing cell bodies in the background. Bars: 100 µm.

Biocytin is a powerful tracer for visualizing connections with histological techniques. In a previous paper (Mishra et al., 2009) we have shown that both kinds of modified biocytin, aminopropyl and serine biocytin, are well suited for tracing and have, in addition, the advantage of being considerably more stable than the biocytin itself. We further investigated the post-mortem tissue sections of the same MR experimental animals. However, no stain could be seen in the case of [**Gd.L²**], and in case of **[Gd.L¹]** the stain was restricted to places where the concentration is usually strongest, i.e. to the injection site and the striatum bundles (Figure 6). This could be explained by an impaired reaction with the avidin peroxidase-DAB (3,3′-Diaminobenzidine) cocktail, necessary for histological staining. This can be concluded from the fact that our *in vitro* uptake studies on N18 murine neuroblastoma cells clearly revealed that these probes were taken up well by neurons even at low concentrations. The lower modulation of proton longitudinal relaxivity upon avidin binding of [**Gd.L¹**] and [**Gd.L²**] (assuming a 2:1 stoichiometry of interaction) suggested that the interaction with avidin was strongly impaired. To further rule out the lack of uptake and/or transport and support the MRI findings, similar behavior was obtained after *in vivo* injections of [**Fluo.L¹**] into the primary motor cortex (M1) of anaesthetized albino rats and

evaluation of the transport of this compound 24 h post-injection. We observed by fluorescence microscopy that [**Fluo.L^1**] had been taken up by neurons (Figure 7), but we could not detect any stain in the same section using the staining technique depending on the biotin-avidin peroxidase-DAB (3,3'-Diaminobenzidine) cocktail.
It is conceivable that the modifications introduced in the model modified biocytin (aminopropyl and serine biocytin) described above, together with the significant increase in molecular weight by about a factor of 2.5, sterically hinder the staining with avidin peroxidase-DAB cocktail in cells substantially, but retain the uptake and transport properties of the resulting contrast agent.

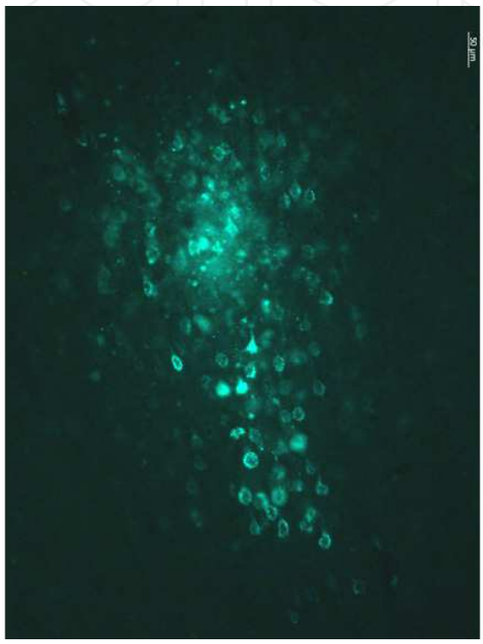

Fig. 7. Injection site in the motor cortex of a rat, 24 h after injection with **[Fluo.L^1].**
It can be seen that the neurons have taken up the tracer. Under transmission light, no stain could be seen, although the same section had undergone an avidin-biotin reaction. Bar 50 µm.

3. Conclusion

In summary, we present data on the functionalization of biocytin, a well known neuronal tract tracer, and demonstrate the validity of the approach by showing cortical connectivity in live rats with the help of MRI. Our study offers a new platform for the development of multimodal molecular imaging tools for brain connectivity studies *in vivo*.

4. Materials and methods

4.1 Chemicals

All solvents and reagents were purchased at analytical grade from commercial suppliers (Acros, Aldrich, Fluka, Merck, Strem and VWR) and were used without further purification unless otherwise stated. All air- or water-sensitive chemicals were stored under an inert atmosphere. Ultra pure de-ionised water (18 MΩ cm^{-1}) was used throughout.

4.2 Chromatography

Flash column chromatography was performed using flash silica gel 60 (70-230 mesh) from Merck. Thin layer chromatography (TLC) was performed on aluminum sheet silica gel plates with 0.2 mm thick silica gel 60 F_{254} (E. Merck) using different mobile phases. The compounds were visualized by UV irradiation (254 nm) or iodine staining. Reverse phase HPLC was performed at room temperature on a Varian PrepStar Instrument, equipped with PrepStar SD-1 pump heads. UV absorbance was measured using a ProStar 335 photodiode array detector at 214 nm. Analytical RP-HPLC was performed in a stainless steel Chromsep (length 250 mm, internal diameter 4.6 mm and particle size 8 μm) C_{18} column and semi-preparative RP-HPLC was performed on a stainless steel Chromsep (length 250 mm, internal diameter 21.2 mm and particle size 5 μm) C_{18} column (Varian). The compounds were purified using one of the following two methods. Method A: gradient with the mobile phase starting from 95% solvent A (H_2O) and 5% of solvent B (MeOH) to 70% B in 10 min, 90% B in 18 min, 90% B isocratic till 24 min and decreased to 5% B in 28 min. Method B: 95% solvent A (H_2O, 0.1% HCOOH) and 5% solvent B (acetonitrile, 0.1% HCOOH) to 70% solvent B in 10 min and then to 100% in the next 8 min running isocratic for 12 min and then back to 5% solvent B in the next 2 min. The flow rate generally used for analytical HPLC was 1 mL/min and for semi-preparative HPLC 15 mL/min. All the HPLC-grade solvents for HPLC were filtered through a nylon-66 Millipore filter (0.45 μm) prior to use.

4.3 Spectroscopy

^{1}H NMR and ^{13}C NMR spectra were recorded on Bruker DRX250 and DRX400 spectrometers at room temperature. The ^{1}H NMR chemical shifts were adjusted to the residual protons of the solvent peaks which were referenced to TMS (0.0 ppm), and ^{13}C NMR chemical shifts were referenced to $CDCl_3$ (77.0 ppm).

Electrospray ionization mass spectra (ESI-MS in positive and negative ion mode) were performed on an ion trap SL 1100 system (Agilent) and High Resolution (HR) mass spectra were measured on Bruker Daltonics Apex II FT-ICR-MS (Bruker).

Inductively coupled plasma optical emission spectrometry (ICP-OES) for the evaluation of the Gd^{3+} concentration was performed using a Jobin–Yvon Ultima 2 spectrometer.

4.4 *In vitro* MR tube measurements

Longitudinal and transverse relaxation times (T_1 and T_2) of the [**Gd.L^1**] and [**Gd.L^2**] were examined using a vertical 7T (300 MHz)/60-cm diameter bore magnet (Bruker BioSpin). Four different concentrations (1 mM, 0.75 mM, 0.5 mM, 0.25 mM) of [**Gd.L^1**] and [**Gd.L^2**] were prepared in Phosphate-Buffered-Saline (PBS) in 1.5 mL Eppendorf tubes at physiological pH to measure relaxivity. Each tube was filled with 400 µl of the CA solution. The y-axis intercept of the linear regression plot of the relaxation rate obtained for these tubes with the corresponding concentration of CA gave the diamagnetic relaxation rate ($1/T_d$).

To measure the changes in r_1 and r_2 upon binding to avidin, MRI experiments were performed with increasing concentrations of avidin proportional to a constant concentration of [**Gd.L^1**] and [**Gd.L^2**] (0.25 mM) incubated for 1 h at 37°C. The stock solution of avidin (1 mM) was prepared in PBS at pH 7.4.

Axial images were obtained for the set of tubes at 7T and the T_1/T_2 values were then calculated.
Relaxivity at different concentrations of avidin was then calculated using equation [1].

$$r_{1,obs} = (1/T_{1,obs}\text{-}1/T_{1,d}) \,/\, [\mathrm{Gd.L^n}] \quad (1)$$

where $T_{1,obs}$ is the measured T_1, $T_{1,d}$ is the diamagnetic contribution of the solvent (calculated to be 2400 - 2700 ms) and [GdL^n] is the concentration in mmol/L of the appropriate Gd(III) complex (n = 1-2).

4.5 Synthesis of ligands and tracers

(*S*)-methyl 3,15-dioxo-10-(5-((3a*R*,4*R*,6a*S*)-2-oxo-hexahydro-1*H*-thieno[3,4-*d*]imidazol-4-yl)pentanoyl)-1-phenyl-16-(4,7,10-tris(2-*tert*-butoxy-2-oxoethyl)-1,4,7,10-tetraazacyclododecan-1-yl)-2-oxa-4,10,14-triazahexadecane-5-carboxylate (7). A solution of compound **6** (0.3 g, 0.52 mmol), NMM (0.12 mL, 1.0 mmol) and HOBt (0.11 g, 0.57 mmol) in anhydrous DMF (15 mL) was stirred at 0-5˚C for 15 min and then EDC (0.08 g, 0.57 mmol) was added. The reaction mixture was stirred overnight at room temperature. Completion of the reaction was verified by ESI-MS, the solution was poured into water (50 mL) and extracted with EtOAc (3 x 50 mL). The combined organic layers were dried over anhydrous Na_2SO_4, filtered and the filtrate evaporated under reduced pressure. The residue was purified by column chromatography (silica gel, 10% MeOH in CH_2Cl_2, R_f = 0.15) to give **7** as a yellow gum (0.28 g, 48%). ^{1}H NMR ($CDCl_3$, 250 MHz), δ (ppm): 1.10-1.30 (m, 2H); 1.42 (s, 18H); 1.52 (s, 10H); 1.60-1.95 (m, 12H); 2.03 (br s, 2H); 2.34 (br s, 3H); 2.62-2.99 (m, 6H); 3.32-3.94 (m, 20H); 3.76 (br s, 6H); 3.94-3.98 (m, 2H); 4.23-4.43 (m, 2H); 4.47-4.63 (m, 1H); 5.12 (s, 2H); 5.48-5.77 (m, 1H); 7.29-7.43 (m, 5H). ESI-MS (+): calcd $C_{56}H_{93}N_9O_{13}S$: m/z 1133.5 $(M+H)^+$; found 1133.2 $(M+H)^+$.

[4,7-Bis-carboxymethyl-10-(2-(3-(*N*-((*S*)-5-amino-5-carboxypentyl)-5-((3a*R*,4*R*,6a*S*)-2-oxo-hexahydro-1H-thieno[3,4-d]imidazol-4-yl)pentanamido)propylamino)-2-oxoethyl)-1,4,7,10-tetraaza-cyclododec-1-yl]-acetic acid (L^1). A solution of compound **7** (0.25 g, 0.22 mmol), 10% Pd-C (0.07 g) and H_2 (50 psi) in MeOH (20 mL) was stirred at room temperature in Parr-apparatus for 8 h. Completion of the reaction was verified by ESI-MS, the solution was filtered through a G-4 sintered funnel, and the filtrate was evaporated under reduced pressure. This crude product was further dissolved in TFA (20 mL) and stirred overnight at room temperature. TFA was evaporated under reduced pressure. A solution of crude product in THF:MeOH:water (3:2:2) (10 mL) was stirred at 0-5˚C for 15 min and then LiOH (0.11 g, 4.7 mmol) was added. The reaction mixture was stirred for 2 h at room temperature. Completion of the reaction was verified by ESI-MS, the solvent was evaporated under reduced pressure and the residue was purified by preparative HPLC (t_R = 3.8 min). After lyophilization, **L^1** was obtained as a light yellow sticky solid (0.1 g, 56%). ^{1}H NMR (D_2O, 250 MHz), δ (ppm): 1.20-2.16 (m, 16H); 2.47 (t, *J*=7.0 Hz, 2H); 2.70-3.90 (br. m, 32H); 4.40-4.53 (m, 1H); 4.24-4.28 (m, 1H). ^{13}C NMR (D_2O, 62.9 MHz), δ (ppm): 24.9; 27.8; 28.2; 30.5; 30.9; 32.8; 35.0; 39.7; 42.4; 46.2; 47.9; 48.4; 50.7; 50.9; 51.2; 53.2; 53.8; 57.1; 58.1; 58.6; 63.0; 64.8; 164.2; 165.3; 167.2; 177.1; 178.0; 178.8. ESI-MS (+): calcd $C_{35}H_{61}N_9O_{11}S$: m/z 816.4 $(M+H)^+$; found 816.3 $(M+H)^+$.

Methyl 2-(benzyloxycarbonylamino)-3-bromopropanoate (8). *N*-carbobenzyloxy-L-serine methyl ester (2 g, 8 mmol) and PPh_3 (4 g, 16 mmol) were added in 50 ml anhydrous DMF.

Finally *N*-bromosuccinimide (2.8 g, 16 mmol) was added in small aliquots to the reaction mixture. The mixture was stirred for 30 minutes at 50 °C. Heating bath was removed and 2 ml of MeOH was added to quench the reaction. 100 ml of ether was added and the reaction mixture was extracted with 100 ml water. The organic layer was dried over anhydrous Na_2SO_4, concentrated under vacuum and purified by column chromatography (silica gel, 30% EtOAc in n-hexane) to give **8** as a yellow gum (2.1 g, 84%). ^{1}H NMR ($CDCl_3$, 400 MHz), δ (ppm): 3.40-3.70 (m, 5H); 4.57-4.62 (m, 1H); 4.91 (s, 2H); 5.49-5.58 (m, 1H); 7.07-7.28 (m, 5H). ^{13}C NMR ($CDCl_3$, 100 MHz), δ (ppm) 33.6; 53.0; 54.2; 67.2; 128.0; 128.2; 128.4; 139.5; 159.5; 169.2. ESI-MS (+): calcd $C_{12}H_{14}BrNO_4$: m/z 317.1 $(M+H)^+$ and found 317.3 $(M+H)^+$.

Methyl 2-(benzyloxycarbonylamino)-3-(1,4,7,10-tetraazacyclododecan-1-yl)propanoate (9). Compound **8** (0.6 g, 1.9 mmol) in 25 ml of toluene was added dropwise to the solution of cyclen (2g, 11.6 mmol) in 100 ml of toluene at room temperature. The reaction mixture was refluxed for 18 h. The reaction mixture was cooled, filtered through a G-4 sintered funnel; filtrate was evaporated under reduced pressure, dissolved in 200 ml CH_2Cl_2, extracted from the water (4x100 ml). The organic layers were combined, dried over anhydrous Na_2SO_4 and then concentrated under vacuum to obtain the product with cyclen. The residue was purified by column chromatography (silica gel, 10% MeOH in CH_2Cl_2) to give **9** as colorless oil (0.34 g, 44%). ^{1}H NMR ($CDCl_3$, 250 MHz), δ (ppm): 2.20-3.02 (m, 18H); 3.69 (s, 3H); 4.36 (br s, 1H); 5.02 (s, 2H); 5.07-5.25 (m, 4H); 7.25-7.40 (m, 5H). ^{13}C NMR ($CDCl_3$, 62.9 MHz), δ (ppm) 43.5; 52.5; 53.2; 53.7; 53.9; 55.0; 59.9; 66.3; 127.7; 128.9; 132.1; 134.2; 161.4; 176.8. ESI-HRMS (+): calcd $C_{20}H_{33}N_5O_4$: m/z 408.2605 $(M+H)^+$; found 408.2607 $(M+H)^+$.

[4,7-Bis-butoxycarbonylmethyl-10-(2-(benzyloxycarbonylamino)-3-methoxy-3-oxopropyl -1,4,7,10-tetraaza-cyclododec-1-yl]-acetic acid *tert*-butyl ester (10). A solution of compound **9** (4.1 g, 10.1 mmol) and sodium carbonate (6.4 g, 60.0 mmol) was added in 70 ml MeCN (dry) and heated at 60 °C for 1 h. The reaction mixture was cooled and *tert*–butylbromoacetate (5.29 ml, 27.1 mmol) in MeCN (25 ml) was added dropwise. The mixture was then refluxed for 6 h. It was then filtered through a G-4 sintered funnel, washed with MeCN and concentrated under vacuum. The obtained residue was taken in CH_2Cl_2 (100 ml) and extracted with water (2x50 ml). The organic layer was dried over anhydrous Na_2SO_4 and concentrated to yellow oil. The residue was purified by column chromatography (silica gel, 5% MeOH in CH_2Cl_2) to give **10** as light yellow solid (3.5 g, 72%). ^{1}H NMR ($CDCl_3$, 250 MHz), δ (ppm): 1.32 (s, 9H); 1.39 (s, 18H); 1.83-2.56 (m, 8H); 2.60-3.50 (m, 16H); 3.66 (s, 3H); 4.47 (br s, 1H); 4.71 (br s, 1H); 5.24 (s, 2H); 7.16-7.42 (m, 5H). ^{13}C NMR ($CDCl_3$, 62.9 MHz), δ (ppm): 27.8; 28.0; 50.3; 50.5; 51.3; 52.3; 52.6; 53.3; 55.5; 56.1; 56.5; 66.9; 82.1; 82.4; 127.7; 127.9; 128.3; 135.9; 157.0; 171.8; 172.7; 173.1. ESI-HRMS (+): calcd $C_{38}H_{63}N_5O_{10}$: m/z 750.4647 $(M+H)^+$; found 751.4641 $(M+H)^+$.

2-(benzyloxycarbonylamino)-3-(4,7,10-tris(2-*tert*-butoxy-2-oxoethyl)-1,4,7,10-tetraazacyclododecan-1-yl)propanoic acid (11). A solution of compound **10** (0.1 g, 0.13 mmol) was stirred in 7 mL of THF:MeOH:water (3:2:2) at 0-5˚C for 15 min and then LiOH (6.5 mg, 0.27 mmol) was added. The reaction mixture was stirred for 2 h at room temperature. The progress of the reaction was checked by ESI-MS. After completion, the reaction mixture was concentrated under reduced pressure and **11** was obtained as white powder (0.76 g, 64%). ^{1}H NMR ($CDCl_3$, 250 MHz), δ (ppm): 1.32 (s, 9H); 1.39 (s, 18H); 1.83-2.56 (m, 8H); 2.60-3.50 (m, 16H); 4.47 (br s, 1H); 4.71 (br s, 1H); 5.24 (s, 2H); 7.16-7.42 (m, 5H). ^{13}C NMR ($CDCl_3$, 62.9 MHz), δ (ppm): 27.8; 28.0; 50.3; 50.5; 52.3; 52.6; 53.3; 55.5; 56.1; 56.5; 66.9; 82.1; 82.4; 127.7; 127.9; 128.3; 135.9; 157.0; 171.8; 172.7; 173.1. ESI-MS (+): calcd $C_{37}H_{61}N_5O_{10}$: m/z 736.9 $(M+H)^+$; found 737.1 $(M+H)^+$.

[4,7-Bis-butoxycarbonylmethyl-10-(2-(benzyloxycarbonylamino)-3-((*R*)-5-(*tert*-butoxycarbonylamino)-6-methoxy-6-oxohexylamino)-3-oxopropyl-1,4,7,10-tetraaza-cyclododec-1-yl]-acetic acid *tert*-butyl ester (12). Compound 11 (0.29 g, 0.4 mmol) was dissolved in DMF (5 ml, dry) and NMM (0.1 ml, 0.9 mmol), EDC (0.086 g, 0.44 mmol) and (*R*)-methyl 6-amino-2-(*tert*-butoxycarbonylamino)hexanoate (0.16 mmol, 0.6 mmol) were added under N_2 atmosphere. The reaction mixture was stirred at 60°C for 1h. Thereafter, HOBt (0.06 g, 0.44 mmol) was added and the heating was continued for 3 h. DMF was evaporated under reduced pressure and the obtained residue was dissolved in EtOAc. The organic layer was washed with water, dried under anhydrous Na_2SO_4, and concentrated under reduced pressure to obtain crude yellowish residue. This was purified by column chromatography (silica gel, 5% MeOH in CH_2Cl_2) to obtain 12 as yellowish solid (46%, 0.18 g). ^{1}H NMR (300 MHz, $CDCl_3$), δ (ppm): 1.20 - 1.54 (m, 38 H), 1.54 - 1.88 (m, 5 H), 1.87 - 2.65 (m, 9 H), 2.64 - 3.12 (m, 8 H), 3.12 - 3.52 (m, 6 H), 3.69 - 3.81 (m, 3 H), 4.15 - 4.32 (m, 1 H), 4.67 (br. s., 1 H), 4.91 - 5.37 (m, 2 H), 7.19 - 7.44 (m, 5 H). ^{13}C NMR (75 MHz, $CDCl_3$), δ (ppm): 22.7, 27.8, 27.9, 28.0, 28.2, 28.8, 31.9, 38.8, 49.9, 52.0, 53.3, 53.5, 55.4, 56.3, 56.4, 66.1, 79.4, 81.8, 81.9, 82.3, 127.3, 127.4, 128.1, 136.8, 155.4, 157.0, 171.8, 172.0, 173.3. ESI-MS (+): calcd $C_{49}H_{83}N_7O_{13}$: *m/z* 978.6 $(M+H)^+$; found 978.5 $(M+H)^+$.

[4,7-Bis-butoxycarbonylmethyl-10-(2-amino-3-((*R*)-5-(*tert*-butoxycarbonylamino)-6-methoxy-6-oxohexylamino)-3-oxopropyl-1,4,7,10-tetraaza-cyclododec-1-yl]-acetic acid *tert*-butyl ester (13). Compound **12** (0.05 g, 0.05 mmol) was dissolved in ethanol (10 ml) and Pd-C (0.005 g, 10% w/w) was suspended. The mixture was stirred in a Parr aparatus under H_2 atmosphere (3 atm) for 4 h. The solvent was evaporated under reduced pressure to obtain the product **13** as yellowish oil in quantitative yield. ^{1}H NMR (300 MHz, $CDCl_3$), δ (ppm): 1.18 - 1.36 (m, 5 H), 1.36 - 1.41 (m, 11 H), 1.41 - 1.46 (m, 23 H), 1.49 - 1.58 (m, 2 H), 1.58 - 1.67 (m, 1 H), 1.69 - 1.85 (m, 1 H), 1.93 - 2.35 (m, 4 H), 2.42 - 2.77 (m, 6 H), 2.76 - 3.02 (m, 6 H), 3.08 - 3.39 (m, 7 H), 3.40 - 3.53 (m, 1 H), 3.68 (s, 3 H), 4.15 - 4.21 (m, 1 H). ^{13}C NMR (75 MHz, $CDCl_3$), δ (ppm): 22.7, 27.9, 28.1, 28.3, 28.8, 32.0, 39.3, 49.9, 51.2, 52.2, 53.5, 55.4, 56.8, 57.8, 79.6, 81.6, 81.9, 82.5, 155.5, 167.67, 167.75, 170.7, 173.4. ESI-MS (+): calcd $C_{41}H_{77}N_7O_{11}$: *m/z* 844.6 $(M+H)^+$; found 844.5 $(M+H)^+$.

[4,7-Bis-carboxymethyl-10-(3-((*R*)-5-amino-5-carboxypentylamino)-3-oxo-2-(5-((3a*S*,4*S*,6a*R*)-2-oxo-hexahydro-1*H*-thieno[3,4-*d*]imidazol-4-yl)pentanamido)propyl)-1,4,7,10-tetraaza-cyclododec-1-yl]-acetic acid (L^2). Compound **13** (0.045 g, 0.053 mmol) was dissolved in anhydrous DMF (2 ml) and HATU (0.022 g, 0.058 mmol) and DIPEA (0.019 ml, 0.1 mmol) were added under inert atmosphere. The reaction mixture was stirred at room temperature for 18 h. The formation of **14** was confirmed by ESI-MS, the solvent was evaporated under reduced pressure and the residue was redissolved in ethylacetate and washed with water. The collected organic layer was dried with anhydrous Na_2SO_4 and evaporated under reduced pressure till dry. The residue was subjected to global deprotection. Methyl ester hydrolysis was carried out by LiOH (0.13 mmol, 0.005 g) in THF:MeOH:H_2O (3:3:2) for 2h. The solvent was evaporated and the residue dissolved in TFA (10 ml, neat) to hydrolyze *tert*-Bu-ester and deprotect the Boc group. TFA was evaporated under reduced pressure to obtain a yellowish residue. The residue was redissolved in water, the pH was increased to 7 and thereafter purified by RP-HPLC (t_R = 4.8) to obtain the product, **L^2**, as a yellow sticky solid. ^{1}H NMR (300 MHz, D_2O), δ (ppm): 1.33 (br. s., 4 H), 1.42 - 1.60 (m, 5 H), 1.60 - 1.72 (m, 1 H), 1.74 - 1.92 (m, 2 H), 2.16 - 2.38 (m, 2 H), 2.65 - 2.96 (m, 6 H), 2.98 - 3.36 (m, 13 H), 3.41 - 3.60 (m, 3 H), 3.62 (s, 1 H), 3.64 - 3.82 (m, 4 H), 3.84 - 4.03 (m, 3 H), 4.25 - 4.33 (m, 1 H), 4.36

(dd, *J*=7.88, 4.58 Hz, 1 H), 4.53 (dd, *J*=7.63, 5.09 Hz, 1 H). ^{13}C NMR (75 MHz, D_2O), δ (ppm): 20.8, 20.9, 23.9, 24.0, 26.9, 27.2, 27.3, 29.0, 34.0, 38.1, 38.9, 46.8, 48.5, 49.9, 51.5, 52.4, 52.8, 53.2, 54.58, 54.68, 55.1, 55.8, 59.4, 61.2, 149.9, 164.5, 173.0, 176.8. Compound 14: ESI-MS (+): calcd $C_{51}H_{91}N_9O_{13}S$: m/z 1070.6 $(M+H)^+$; found 1070.5 $(M+H)^+$. Compound L²: ESI-MS (-): calcd $C_{33}H_{57}N_9O_{11}S$: m/z 786.4 $(M-H)^-$; found 786.4 $(M-H)^-$.

General Preparation of Gadolinium Complexes of L¹ and L². Gadolinium complexes of **L¹** and **L²** were prepared from corresponding solutions of the ligands (1 eq) and solutions of $GdCl_3.6H_2O$ (1.1 eq). The reaction mixture was stirred at 60°C for 20 h. The pH was periodically checked and adjusted to 6.5 using solutions of NaOH (1 M) and HCl (1 N) as needed. After completion, the reaction mixture was cooled and passed through chelex-100 to trap free Gd^{3+} ions, and the Gd-loaded complexes were eluted. The absence of free Gd^{3+} was checked with xylenol orange indicator. The fractions were lyophilized to obtain off-white solids. These complexes were characterized by ESI-MS in positive and negative mode and the appropriate isotope pattern distributions for Gd^{3+} were recorded.

[Gd.L¹]. ESI-MS (+): calcd $C_{35}H_{58}{}^{155}GdN_9O_{11}S$: m/z 971.3 $[M+H]^+$; found 971.4 $[M+H]^+$, r_{1p} = 5.52 $[mM^{-1}s^{-1}]$ at 300 MHz.

[Gd.L²]. ESI-MS (+): calcd $C_{33}H_{54}{}^{155}GdNaN_9O_{11}S$: m/z 965.2 $[M+Na]^+$; found 965.3 $[M+Na]^+$, r_{1p} = 7.27 $[mM^{-1}s^{-1}]$ at 300 MHz.

4.6 *In vitro* cell studies of [Gd.L¹], [Gd.L²] and [Fluo-L¹]

4.6.1 Cell culture

N18 mouse neuroblastoma cells (kind gift of Prof. Bernd Hamprecht, University of Tübingen, Germany) were cultured as a monolayer at 37°C with 5% CO_2 in antibiotic free Dulbecco's Modified Eagle's Medium (DMEM) supplemented with 10% fetal bovine serum (FBS) and 4 mM L-glutamine, (all purchased from Biochrom AG). Cells were passaged by trypsinization with trypsin/EDTA 0.05/0.02% (w/v) in phosphate-buffered saline (PBS; Biochrom AG, Germany) for 5 minutes every second to third day. Prior to experiments the serum content was stepwise reduced to 0.625% to induce morphological differentiation.

4.6.2 Preparation of labeling solutions

CA were dissolved in water and the concentration was determined by BMS measurement for **[Gd.L¹]** and **[Gd.L²]** or by absorbance of fluorescein for [**Fluo.L¹**]. For each experiment, dilutions from these stocks were freshly made in incubation medium and thoroughly mixed at indicated concentrations.

4.6.3 Live cell imaging

Microscopy was done in single channel Ibidi slides (Ibidi GmbH, Germany) by inoculation of N18 cells (3 x 10^5 cells/ml) cultured in Dulbecco's Modified Eagle's Medium supplemented with 0.625% fetal bovine serum and 4 mM L-glutamine (all purchased from Biochrom AG). After reaching 70-80% confluency, cells were incubated with 50 μM of [**Fluo.L¹**] for 12 hours. Before washing cells were incubated with nuclear stain Bisbenzimid 33342 (Hoechst 33342) for 5 min. Afterwards, extracellular fluorescence was quenched by the addition of ice-cold Trypan Blue for 3 min (Rennert et al.). After repeated cell washings with Hank's buffered saline solution (HBSS, Biochrom AG, Germany), fluorescence microscopy was performed on a Zeiss Axiovert 200M (Carl Zeiss AG, Germany) with a Plan-Apochromat 63X objective to observe the cellular localization of [**Fluo.L¹**]. The imaging

conditions were kept constant for the observation of different samples. Cellular localization and distribution of [**Fluo.L¹**] was determined by irradiating with blue light (470 nm) and observing at 525 nm, and nuclear labeling by Hoechst was imaged at 460 nm. Also phase contrast images with Differential Interference Contrast (DIC) of the same area were made to detect if the cells maintain their normal morphology in the presence of compound.

4.6.4 MR measurement in cells

For MR imaging, serum deprived N18 cells (1.25% FBS) were cultured in 175 cm^2 tissue culture flasks and labeled with 20 or 40 µM of **[Gd.L¹]** or **[Gd.L²]** in HBSS/10mM HEPES for 6h. After incubation samples of the treatment solution were collected, if required centrifuged, and 500 µl were used for determination of R_1 and R_2. Cells were repeatedly washed with HBSS, trypsinized, centrifuged and re-suspended in 0.5 ml Eppendorf tubes at a cell density of 1 x 10^7/500µl in complete medium. Cells were allowed to settle before MR measurements. Tubes with medium only and cells without CA were used as controls. Two tubes of treatment solutions, HBSS/10 mM HEPES as well as of cells for each condition were used. Experiments were done at least twice.

MR imaging of the cell pellets at room temperature (~21 ˚C) was performed in a 3 T (123 MHz) human MR scanner (MAGNETOM Tim Trio, Siemens Healthcare, Germany), using a 12-channel RF Head coil and slice selective measurements from a slice with a thickness of 1 mm positioned through the cell pellet.

T_1 was measured using an inversion-recovery sequence, with an adiabatic inversion pulse followed by a turbo-spin-echo readout. Between 10 and 15 images were taken, with the time between inversion and readout varying from 23 ms to 3000 ms. With a repetition time of 10 s, 15 echoes were acquired per scan and averaged six times. For T_2, a homewritten spin-echo sequence was used with echo times varying from 18 ms to 1000 ms in about 10 steps and a repetition time of 8 s. Diffusion sensitivity was reduced by minimizing the crusher gradients surrounding the refocusing pulse. All experiments scanned 256^2 voxels in a field-of-view of 110 mm in both directions resulting in a voxel volume of 0.43 × 0.43 × 1 mm^3.

Data analysis was performed by fitting to relaxation curves with self-written routines under MATLAB 7.1 R14 (The Mathworks Inc., United States). The series of T_1 relaxation data were fitted to the following equation.

T_1 series with varying $t = T_I$: $S = S_0 (1 - \exp(-t / T_1) + S_{(TI = 0)} \exp(-t / T_1)$.

Nonlinear least-squares fitting of three parameters S_0, $S_{(TI = 0)}$, and T_1 was done for manually selected regions-of-interest with the Trust-Region Reflective Newton algorithm implemented in MATLAB. The quality of the fit was controlled by visual inspection and by calculating the mean errors and residuals.

Evaluation of the signal intensities in the T_1-weighted MR images were performed in ImageJ (http://rsb.info.nih.gov/ij) by defining a circular region of interest (ROI) inside one tube image and measuring the mean signal intensity and standard deviation in the included voxels. Further statistical analyses were performed in GraphPad Prism 5.03 (GraphPad Software, Inc., USA).

4.7 *In vivo* rat experiments

To test whether **[Gd.L¹]**, **[Gd.L²]** and **[Fluo.L¹]** were transported inside cells and could be visualized by MR and histological methods, we performed injections of all three compounds into the primary motor cortex of 8 albino rats (Sprague Dawley). Three of them (with

[Gd.L¹]) were sacrificed after 24 h and the other three (one with **[Gd.L¹]** and two with **[Gd.L²]**) were euthanized after 48 h. The remaining two (with **[Fluo.L¹]**) were euthanized after 24 h.

4.7.1 Injections

All rats were anaesthetized with 2% isoflurane (Abbott) and placed in a stereotaxic frame (Kopf Instruments). After additional use of xylocain for local analgesia in the surgery area, a craniotomy was performed and a pulled fused silica capillary (ID 50µm; OD 150 µm; tip diameter 20-30 µm) was placed in the primary motor cortex at a depth of 1.2 mm below the surface. One compound per animal was then injected using a pressure cell containing the compound attached to the other end of the fused silica capillary. 100 nl of 4% tracer solution was injected at a flow rate of 3.3 nl/min. After injection, the capillary was left in place for 10 minutes before retracting it stepwise to avoid backflow of the injected solution.

In some cases we made iontophoretic injections, using borosilicate pipettes with tip diameters of 20-25 µm. In case of the injection shown in Fig. 6, injection time was 35 min (7s on, 7 s off) with a current of 4 µA. In case of the injection shown in Fig. 7, injection time was 70 min (7 s on, 7 s off) with a current of 10 µA.

At the end of the procedure, the animals received an intraperitoneal injection of analgesics and antibiotics [5mg/kg Baytril® (Bayer) and 2.5mg/kg Finadyne® (Essex)]. The animals to be left for 48 h received another injection of analgesics and antibiotics after 24 h.

4.7.2 *In vivo* MRI experiments

For the MRI experiments, the animals were anaesthetized with 1.5-2% isoflurane and placed in a home-made quadrature coil integrated within a stereotaxic animal holder. The head holder was adapted with movable bite and ear bars and positioned fixed on a magnet chair. This allowed precise positioning of the animal with respect to the coil and the magnet, avoiding movement artifacts. Body temperature, heart rate, CO_2 and SpO_2 were monitored throughout the scanning session. We typically scanned the animals before, immediately after and 24-48 h after the injection of CAs. One scan session consisted on 5 to 7 scans of 18 min each.

Experiments were carried out in a vertical 7T (300 MHz)/60-cm diameter bore magnet (Bruker BioSpin, Ettlingen). The saddle coil, which was designed to generate a homogeneous field over the whole rat brain, was used to transmit and receive. The MR system was controlled by a Bruker BioSpec console (ParaVision 3, 4 and 5 at different time periods) running under Linux operating system. We used a Modified Driven Equilibrium Fourier Transform (MDEFT) method with MDEFT-preparation (Lee et al., 1995) to obtain T_1-weighted anatomical images. The scan parameters were: TR = 22.2 ms, TE = 4.8 ms, FA = 20°, ID = 1000 ms and four segments. The geometric parameters of the 3D scans were: matrix 192×136×100, FOV = 48×34×25 mm and voxel size 0.25×0.25×0.25 mm.

The MRI images were analyzed with custom-developed Matlab functions (v7.5.0, MathWorks). An automated realignment procedure of SPM (statistical parametric mapping, www.fil.ion.ucl.ac.uk) was applied to co-register all scans. For statistical analysis the image intensity was normalized to reference signal intensity in the head muscles. Statistical maps were generated by implementing a Student's t-test (unpaired) at each voxel comparing brain images before and 24-48h after CAs injection. The significant voxels represent the pattern of T_1-weighted MRI signal enhancement induced by the neuronal transport of CAs. The

arbitrary significance threshold was set to $P < 0.01$ (uncorrected for multiple comparisons) for individual voxels, and a minimum cluster size of 3 contiguous voxels constituting at least 3% of total number of voxels for a given region of interest (ROI). The same data were also tested for lower or higher p-values.

4.7.3 Perfusion

After the last MRI session, the animals received a lethal intraperitoneal injection of the barbiturate Pentobarbital sodium (Narcoren from Merial; 2.5 ml/kg body weight). After cessation of all reflexes, the chest of the animal was opened and 0.4 ml of Heparin-Sodium 25000 (ratiopharm) was injected into the heart in order to prevent coagulation. Then a cannula was inserted and the animal was perfused with iosotonic saline (using NaCl 0.9 E from Fresenius) for about 5 minutes and then with the fixative (commercially available 4% paraformaldehyde, phosphate buffered; Roti-Histofix 4% from Carl Roth).
The brain was removed from the skull and kept in the fixative over night. The next day the brain was transferred into 30% sucrose in demineralized water and kept there for at least 4 days until it had sunk. The brain was then sliced into serial sections with a cryotome at a thickness of 70 µm.

4.7.4 Histological procedure

The protocol for the biotin-avidin reaction largely followed that by Horikawa and Armstrong (Horikawa and Armstrong, 1988) with some modifications suggested by Dr. Michaela Schweizer (personal communication). In detail: the sections were collected in phosphate buffer **(**PB, 0.1 M; pH 7.3), rinsed again in PB and then transferred into 1% H_2O_2 in PB for 1 h, in order to block endogenous peroxidase activity. After rinsing 3 times in PB, the sections were kept for 90 min in Triton X-100 (2% in 0.1 M PB from Carl Roth). They were then incubated overnight in avidin-conjugated peroxidase (ABC Elite PK 6100 from Linaris, 1% in 0.1 M PB: i.e. adding 10 drops per 50 µl of each of the two solutions to 49 ml of buffer. Note that the ABC-mixture must stand for 30 min before use). On the next day, the sections were rinsed 2 x 10 min in PB (0.1 M) and then 2 x 10 min in Tris/HCl at pH 7.9 (using a 0.1 M solution of tris-(hydroxymethyl)-aminomethane and pH adjusted to 7.9 with HCl). The sections were then transferred into a solution of diamino benzidine (DAB) and H_2O_2 (DAB tablet were dissolved in demineralized water) for 30 – 45 min. After washing three times in Tris/HCl, the sections were transferred into 0.05 M PB and mounted on electrostatic slides (Superfrost Plus, Menzel, ThermoScientific), air-dried over night, dehydrated in ethanol (70%, 2 x 99%, 1 x 100% ethanol, 2 x terpineole and 2 x xylene), and covered in Eukitt or DePeX.

5. Acknowledgement

The authors thank Prof. Bernd Hamprecht, for the kind gift of the N18 mouse neuroblastoma cell line. The authors also thank Dr. Hellmut Merkle for providing the rf-coil for *in vivo* MRI imaging. This work was supported by the Max-Planck Society and the Hertie Foundation. S.C. acknowledges the support of the Human Frontiers Science Program Organization and the Ministry of Science and Innovation of Spain (BFU2009-09938) and the Consolider-Ingenio 2010 Program (CSD2007-0023). A.M. acknowledges the support of the EC for a Marie Curie IEF (PIEF-GA-2009-237253).

6. References

Aime, S., Botta, M., Parker, D., and Williams, J.A.G. (1996). Extent of hydration of octadentate lanthanide complexes incorporating phosphinate donors: Solution relaxometry and luminescence studies. Journal of the Chemical Society-Dalton Transactions, 17-23.

Baur, B., Suormala, T., and Baumgartner, E.R. (2002). Biocytin and biotin uptake into NB2a neuroblastoma and C6 astrocytoma cells. Brain Res *925*, 111-121.

Bickel, U., Yoshikawa, T., and Pardridge, W.M. (2001). Delivery of peptides and proteins through the blood-brain barrier. Adv Drug Deliv Rev *46*, 247-279.

Botta, M. (2000). Second coordination sphere water molecules and relaxivity of gadolinium(III) complexes: Implications for MRI contrast agents. European Journal of Inorganic Chemistry, 399-407.

Canals, S., Beyerlein, M., Keller, A.L., Murayama, Y., and Logothetis, N.K. (2008). Magnetic resonance imaging of cortical connectivity in vivo. Neuroimage *40*, 458-472.

Canals, S., Beyerlein, M., Merkle, H., and Logothetis, N.K. (2009). Functional MRI evidence for LTP-induced neural network reorganization. Curr Biol *19*, 398-403.

Cao, R., Gu, Z., Hsu, L., Patterson, G.D., and Armitage, B.A. (2003). Synthesis and characterization of thermoreversible biopolymer microgels based on hydrogen bonded nucleobase pairing. J Am Chem Soc *125*, 10250-10256.

Caravan, P., Ellison, J.J., McMurry, T.J., and Lauffer, R.B. (1999). Gadolinium(III) Chelates as MRI Contrast Agents: Structure, Dynamics, and Applications. Chem Rev *99*, 2293-2352.

Caswell, K.K., Wilson, J.N., Bunz, U.H., and Murphy, C.J. (2003). Preferential end-to-end assembly of gold nanorods by biotin-streptavidin connectors. J Am Chem Soc *125*, 13914-13915.

Chandra, S.V., Shukla, G.S., Srivastava, R.S., Singh, H., and Gupta, V.P. (1981). An exploratory study of manganese exposure to welders. Clin Toxicol *18*, 407-416.

Chklovskii, D.B., Mel, B.W., and Svoboda, K. (2004). Cortical rewiring and information storage. Nature *431*, 782-788.

Heller, A.J., Stanley, C., Shaia, W.T., Sismanis, A., Spencer, R.F., and Wolf, B. (2002). Localization of biotinidase in the brain: implications for its role in hearing loss in biotinidase deficiency. Hear Res *173*, 62-68.

Horikawa, K., and Armstrong, W.E. (1988). A versatile means of intracellular labeling: injection of biocytin and its detection with avidin conjugates. J Neurosci Methods *25*, 1-11.

Hymes, J., and Wolf, B. (1996). Biotinidase and its roles in biotin metabolism. Clin Chim Acta *255*, 1-11.

King, M.A., Louis, P.M., Hunter, B.E., and Walker, D.W. (1989). Biocytin: a versatile anterograde neuroanatomical tract-tracing alternative. Brain Res *497*, 361-367.

Kita, H., and Armstrong, W. (1991). A biotin-containing compound N-(2-aminoethyl)biotinamide for intracellular labeling and neuronal tracing studies: comparison with biocytin. J Neurosci Methods *37*, 141-150.

Kobbert, C., Apps, R., Bechmann, I., Lanciego, J.L., Mey, J., and Thanos, S. (2000). Current concepts in neuroanatomical tracing. Prog Neurobiol *62*, 327-351.

Koretsky, A.P., and Silva, A.C. (2004). Manganese-enhanced magnetic resonance imaging (MEMRI). NMR Biomed *17*, 527-531.

Lapper, S.R., and Bolam, J.P. (1991). The anterograde and retrograde transport of neurobiotin in the central nervous system of the rat: comparison with biocytin. J Neurosci Methods *39*, 163-174.

Lee, J.H., Garwood, M., Menon, R., Adriany, G., Andersen, P., Truwit, C.L., and Ugurbil, K. (1995). High contrast and fast three-dimensional magnetic resonance imaging at high fields. Magn Reson Med *34*, 308-312.

Leergaard, T.B., Bjaalie, J.G., Devor, A., Wald, L.L., and Dale, A.M. (2003). In vivo tracing of major rat brain pathways using manganese-enhanced magnetic resonance imaging and three-dimensional digital atlasing. Neuroimage *20*, 1591-1600.

Livramento, J.B., Weidensteiner, C., Prata, M.I., Allegrini, P.R., Geraldes, C.F., Helm, L., Kneuer, R., Merbach, A.E., Santos, A.C., Schmidt, P., *et al.* (2006). First in vivo MRI assessment of a self-assembled metallostar compound endowed with a remarkable high field relaxivity. Contrast Media Mol Imaging *1*, 30-39.

Marchisio, P.C., Weber, K., and Osborn, M. (1979). Identification of multiple microtubule initiating sites in mouse neuroblastoma cells. Eur J Cell Biol *20*, 45-50.

McMillan, D.E. (1999). A brief history of the neurobehavioral toxicity of manganese: some unanswered questions. Neurotoxicology *20*, 499-507.

Mishra, A., Dhingra, K., Schüz, A., Logothetis, N.K., and Canals, S. (2009). Improved Neuronal Tract Tracing with Stable Biocytin-Derived Neuroimaging Agents. ACS Chemical Neuroscience *1*, 129-138.

Mock, D.M., Lankford, G.L., Widness, J.A., Burmeister, L.F., Kahn, D., and Strauss, R.G. (1999). Measurement of circulating red cell volume using biotin-labeled red cells: validation against 51Cr-labeled red cells. Transfusion *39*, 149-155.

Murayama, Y., Weber, B., Saleem, K.S., Augath, M., and Logothetis, N.K. (2006). Tracing neural circuits in vivo with Mn-enhanced MRI. Magn Reson Imaging *24*, 349-358.

Pal, P.K., Samii, A., and Calne, D.B. (1999). Manganese neurotoxicity: a review of clinical features, imaging and pathology. Neurotoxicology *20*, 227-238.

Pautler, R.G., Silva, A.C., and Koretsky, A.P. (1998). In vivo neuronal tract tracing using manganese-enhanced magnetic resonance imaging. Magn Reson Med *40*, 740-748.

Pispa, J. (1965). Animal biotinidase. Ann Med Exp Biol Fenn *43*, Suppl 5:1-39.

Pope, S.J., Kenwright, A.M., Heath, S.L., and Faulkner, S. (2003). Synthesis and luminescence properties of a kinetically stable dinuclear ytterbium complex with differentiated binding sites. Chem Commun (Camb), 1550-1551.

Rivera, V.R., Merrill, G.A., White, J.A., and Poli, M.A. (2003). An enzymatic electrochemiluminescence assay for the lethal factor of anthrax. Anal Biochem *321*, 125-130.

Saleem, K.S., Pauls, J.M., Augath, M., Trinath, T., Prause, B.A., Hashikawa, T., and Logothetis, N.K. (2002). Magnetic resonance imaging of neuronal connections in the macaque monkey. Neuron *34*, 685-700.

Sloot, W.N., and Gramsbergen, J.B. (1994). Axonal transport of manganese and its relevance to selective neurotoxicity in the rat basal ganglia. Brain Res *657*, 124-132.

Suchy, S.F., McVoy, J.S., and Wolf, B. (1985). Neurologic symptoms of biotinidase deficiency: possible explanation. Neurology *35*, 1510-1511.

Tjalve, H., Mejare, C., and Borg-Neczak, K. (1995). Uptake and transport of manganese in primary and secondary olfactory neurones in pike. Pharmacol Toxicol *77*, 23-31.

Tsao, C.Y., and Kien, C.L. (2002). Complete biotinidase deficiency presenting as reversible progressive ataxia and sensorineural deafness. J Child Neurol *17*, 146.

Van der Linden, A., Verhoye, M., Van Meir, V., Tindemans, I., Eens, M., Absil, P., and Balthazart, J. (2002). In vivo manganese-enhanced magnetic resonance imaging reveals connections and functional properties of the songbird vocal control system. Neuroscience *112*, 467-474.

Watanabe, T., Frahm, J., and Michaelis, T. (2004). Functional mapping of neural pathways in rodent brain in vivo using manganese-enhanced three-dimensional magnetic resonance imaging. NMR Biomed *17*, 554-568.

Weizmann, Y., Patolsky, F., Katz, E., and Willner, I. (2003). Amplified DNA sensing and immunosensing by the rotation of functional magnetic particles. J Am Chem Soc *125*, 3452-3454.

Wilbur, D.S., Hamlin, D.K., Vessella, R.L., Stray, J.E., Buhler, K.R., Stayton, P.S., Klumb, L.A., Pathare, P.M., and Weerawarna, S.A. (1996). Antibody fragments in tumor pretargeting. Evaluation of biotinylated Fab' colocalization with recombinant streptavidin and avidin. Bioconjug Chem *7*, 689-702.

Wirsig-Wiechmann, C.R. (1994). Biocytin: a neuronal tracer compatible with rapid decalcification procedures. J Neurosci Methods *51*, 213-216.

Zaffanello, M., Zamboni, G., Fontana, E., Zoccante, L., and Tato, L. (2003). A case of partial biotinidase deficiency associated with autism. Child Neuropsychol *9*, 184-188.

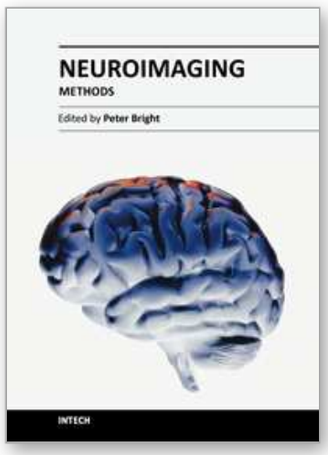

Neuroimaging - Methods
Edited by Prof. Peter Bright

ISBN 978-953-51-0097-3
Hard cover, 358 pages
Publisher InTech
Published online 17, February, 2012
Published in print edition February, 2012

Neuroimaging methodologies continue to develop at a remarkable rate, providing ever more sophisticated techniques for investigating brain structure and function. The scope of this book is not to provide a comprehensive overview of methods and applications but to provide a 'snapshot' of current approaches using well established and newly emerging techniques. Taken together, these chapters provide a broad sense of how the limits of what is achievable with neuroimaging methods are being stretched.

How to reference
In order to correctly reference this scholarly work, feel free to copy and paste the following:

Anurag Mishra, Kirti Dhingra, Ritu Mishra, Almut Schüz, Jörn Engelmann, Michael Beyerlein, Santiago Canals and Nikos K. Logothetis (2012). Biocytin-Based Contrast Agents for Molecular Imaging: An Approach to Developing New In Vivo Neuroanatomical Tracers for MRI, Neuroimaging - Methods, Prof. Peter Bright (Ed.), ISBN: 978-953-51-0097-3, InTech, Available from: http://www.intechopen.com/books/neuroimaging-methods/biocytin-based-contrast-agents-for-molecular-imaging-an-approach-to-developing-new-in-vivo-neuroanat

INTECH
open science | open minds

InTech Europe
University Campus STeP Ri
Slavka Krautzeka 83/A
51000 Rijeka, Croatia
Phone: +385 (51) 770 447
Fax: +385 (51) 686 166
www.intechopen.com

InTech China
Unit 405, Office Block, Hotel Equatorial Shanghai
No.65, Yan An Road (West), Shanghai, 200040, China
中国上海市延安西路65号上海国际贵都大饭店办公楼405单元
Phone: +86-21-62489820
Fax: +86-21-62489821

IntechOpen